Unidirectional emission from a $\mathcal{PT}$-symmetric annular microcavity

Danli Zhu,[1] Shuai Liu,[1] Ruiqin Fan,[1] Shumin Xiao,[1,2] and Qinghai Song[1,2,*]

[1]*State Key Laboratory on Tunable Laser Technology, Ministry of Industry and Information Technology, Key Lab of Micro-Nano Optoelectronic Information System, Shenzhen Graduate School, Harbin Institute of Technology, Shenzhen 518055, China*

[2]*Collaborative Innovation Center of Extreme Optics, Shanxi University, Taiyuan 030006, China*

(Received 1 August 2018; published 25 March 2019)

The introduction of a scattering center to microdisk lasers has been considered as an effective way to tailor their far-field emissions. However, this approach is practically limited by its nearby modes with higher quality (Q) factors and worse directionalities. In this research, by applying the simple concept of parity-time ($\mathcal{PT}$) symmetry, we demonstrate that the resonances with well-designed directionalities can be selectively excited in optical microcavities. Taking the annular microcavities as examples, the unidirectional laser emissions and single-mode operations have been realized simultaneously by breaking the $\mathcal{PT}$ symmetry. More interestingly, we find that the $\mathcal{PT}$-symmetric modulations on the imaginary parts of the refractive index in a circular microdisk can affect the internal ray dynamics and thus generate highly directional laser emission. This research can boost both the fundamental studies and the practical applications of $\mathcal{PT}$-symmetric systems.

DOI: 10.1103/PhysRevA.99.033849

I. INTRODUCTION

Over the past decades, optical microcavities have been intensively studied and gradually become critical platforms for many types of research [1]. In the case of fundamental studies, optical microcavities have been widely used to generate a single photon [2], entangled photon pairs [3], and a polariton laser [4]. On the other hand, optical microcavities are important for practical applications, e.g., add-drop filter [5], modulator [6], optical switches [7], and biological sensors [8–14], for example. Among them, the whispering gallery modes (WGMs) based microcavity is one prominent example. Since the light is trapped by total internal reflection along the cavity boundary for a long time, the cavity quality (Q) factors of the microdisk and microtoroid can be as high as 10^6 and 10^8, respectively [15,16]. As a result, the thresholds of WGM lasers are very low while the accumulated internal laser intensity can be extremely high, making WGM cavities essential for many applications, such as the integrated coherent light source for optical interconnection [17] and active optical sensors [18]. Up to now, WGM lasers have been experimentally demonstrated in semiconductor microdisks [19], silica microtoroids [20,21], silica microspheres [22], and even bottom-up synthesized single crystals [23–25]. In most of these studies, the far-field laser emissions are multiple-directional outputs or nearly isotropic outputs, due to their higher-order rotational symmetry [19–26].

In the past two decades, several types of techniques have been developed to improve the directionalities of WGM lasers [26–28]. Owing to their degrees in both outer and inner boundaries, annular microcavities have been effective platforms for unidirectional outputs. This research was first studied by Apalkov and Raikh in 2004 [29]. After introducing a linear defect away from the microdisk circumference, they theoretically proposed the unidirectional output normal to the cavity boundary. In 2006, Wiersig and Hentschel studied the mode interactions inside the annular dielectric microcavity [30]. By carefully designing the size and position of the inner air hole, the weak coupling occurs between the high-Q WGM and low-Q mode reflected by the inner boundary. As a result, the hybrid mode can combine the high Q factor and unidirectional output and thus overcomes the shortage of low Q factor in Apalkov's design. In 2009, Dettmann [31] and later, others [32,33] further reduced the inner air hole to a point defect and demonstrated the possibility of producing highly directional emission in a single direction. The divergent angle of the output beam can be smaller than 10°. Despite the above theoretical progress, the research on the annular microcavity is practically limited. Typically, there are numerous modes around the designed resonances. However, these modes are less affected by the inner scatter and thus can have worse directionalities but much higher Q factors, making the designed resonances hard to excite experimentally.

The recent progress in $\mathcal{PT}$ symmetry has brought new hope to this research area [34–37]. $\mathcal{PT}$ symmetry was initially proposed in the context of quantum physics to realize a real energy spectrum in a non-Hermitian system. In the optical region, by introducing balanced gain and loss, this concept has been utilized to generate a series of novel photonic devices such as perfect absorbers [38], invisibility [39], laser amplifiers [40], and photonic lattices [41]. Very recently, $\mathcal{PT}$ symmetry started to play important roles in microlasers. After the breaking of $\mathcal{PT}$ symmetry, the output intensities and the resonant wavelengths in circular microdisks, Fabry-Perot microcavities, and coupled cavities have been precisely controlled [42–45]. In this research, we apply $\mathcal{PT}$ symmetry to the annular microcavities and explore its influences on the modifications of internal ray dynamics and the formation of unidirectional emissions.

*qinghai.song@hit.edu.cn

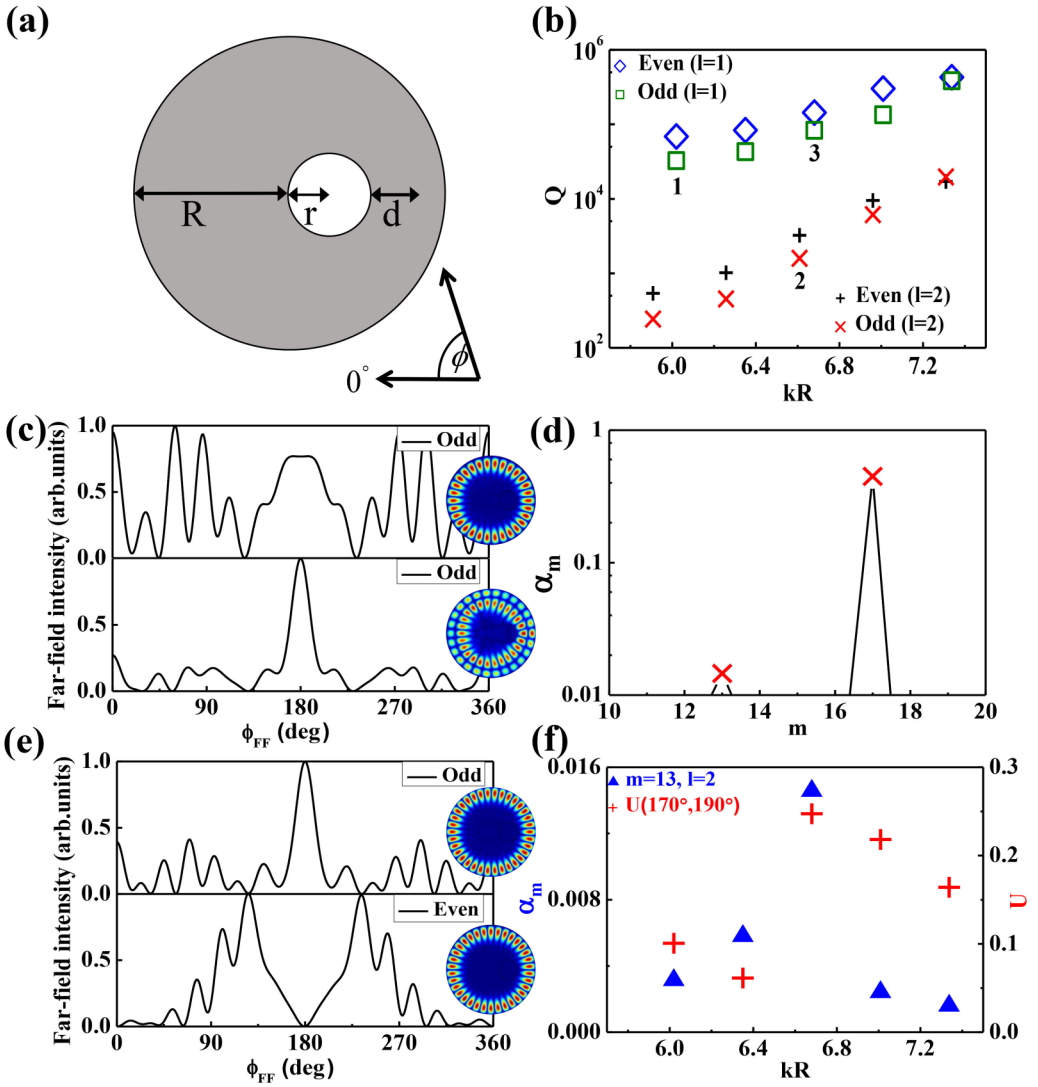

FIG. 1. Mode properties of the annular microdisk. (a) The schematic picture of the annular microcavity. (b) The Q factors of resonances in annular microdisk with $r = 0.22R$ and $d = 0.389R$. (c) The top and bottom panels show the far-field patterns of resonant modes 1 and 2, which are marked in (b). The insets are their field distributions. (d) The angular momentum distributions of the resonance WGM (17, 1) with unidirectional emission. (e) The near-field and far-field patterns of two nearly degenerated WGMs with the same azimuthal number. They correspond to the resonant modes 3 marked in (b). (f) The calculated $U(\theta_1, \theta_2)$ factors and the percentage of components α_m at $m = 13$ of high-Q resonances in (b).

II. RESULTS AND DISCUSSIONS

A. Unidirectional output from annular microdisk

Figure 1(a) illustrates the schematic picture of the annular microcavity. Its geometry is given by the radius R of the large disk, the radius r of the small disk, and the minimal distance d between the disks' circumferences. Following the previous studies, we use a two-dimensional finite-element method (COMSOL MULTIPHYSICS) with effective refractive index n_{eff} to simulate the annular cavity resonances. In our simulation model, the real part of n_{eff} is set as $n = 3.3$ (for InGaAsP) for transverse electric (TE, E is in plane) polarization. For simplicity, the material dispersion is ignored. The surrounding medium is air with $n_0 = 1$. Here, the perfect matching layer (PML) is applied to fully absorb the outgoing waves. Then, the far-field intensity of each mode is recorded by simulating the electromagnetic flux along the inner circle of the PML, which is $15R$ away from the center of the annular microcavity. The Q factors, which are defined as $Q = \text{Re}(\omega)/|2\text{Im}(\omega)|$ (ω is the eigenfrequency), have been summarized in Fig. 1(b) as a function of $kR = \text{Re}(\omega)R/c$. Here k and c are the wave vector and the speed of light in vacuum, respectively, and the structural parameters are fixed at $r = 0.22R$ and $d = 0.389R$. In the following, we analyze the H_z field distributions of the calculated resonant modes by expanding the wave functions inside the cavity in cylindrical harmonics:

$$\psi(\rho, \varphi) = \sum_{m=-\infty}^{\infty} \alpha_m J_m(nk\rho) \exp(im\varphi), \tag{1}$$

where J_m is the mth-order Bessel function of the first kind. Positive and negative values of angular momentum m correspond to the counterclockwise (CCW) and clockwise (CW) propagating components, respectively.

Within a small range of kR, we can see a series of resonant modes with relatively high Q factors in the annular microdisk. Following their field patterns [insets in Fig. 1(c)], these resonances can be categorized into WGMs with different azimuthal numbers (m) and radial numbers (l). Typically, the WGMs with $l = 1$ are confined close to the cavity boundary and are less affected by the inner circle. These resonances thus have higher Q factors and worse directionalities [see far-field patterns in Fig. 1(c) as an example]. On the contrary, the higher-order WGMs are reflected by the inner boundaries and thus produce unidirectional laser emission, which could be clearly seen in the bottom panel of Fig. 1(c). However, their Q factors are typically orders of magnitude lower and hard to excite experimentally.

Interestingly, there are some WGMs with $l = 1$ that can support unidirectional outputs, i.e., modes 3 in Fig. 1(b). The corresponding far-field patterns are shown in Fig. 1(e). In the top panel of Fig. 1(e), a unidirectional beam can be clearly seen around $\phi_{\mathrm{FF}} = 180^{\circ}$. In previous reports, this kind of unidirectional emission is usually explained by the avoided resonance crossing. In optical microcavities, the resonances around the avoided resonance crossing are usually the mixtures of two initial modes and thus can combine their advantages into one hybrid mode. Here, as the resonance is far from the crossing point, a more generic mechanism for unidirectional emission could be expected. Even though the WGM with $l = 1$ is far from the inner circle, its tail along the radial direction which is defined by the Bessel function can still be affected. As a result, the electromagnetic waves are scattered to higher-order orbits. With Eq. (1), the angular distribution α_m of mode 3 [marked in Fig. 1(b)] could be calculated, which is shown in Fig. 1(d). Due to the mirror-reflection symmetry of the microdisk, here we only consider the CCW components. Beside the main peak at $m = 17$, we can also find the other components with $m = 13$. According to the numerical calculations, these azimuthal numbers have radial number $l = 2$ and have much better unidirectional outputs. Considering that the WGMs with $l = 1$ have better light confinement, these components shall dominate the far-field pattern in the top panel of Fig. 1(e). For a direct comparison, we have calculated the percentage of components at $m = 13$ as well as the unidirectionality factor U of all the WGMs with $l = 1$ in Fig. 1(b), where $U(\theta_1, \theta_2)$ relates to the far-field patterns and is defined with $U(\theta_1, \theta_2) = \frac{\int_{\theta_1}^{\theta_2} I(\varphi_{\mathrm{FF}}) d(\varphi_{\mathrm{FF}})}{\int_{-180}^{180} I(\varphi_{\mathrm{FF}}) d(\varphi_{\mathrm{FF}})}$. Here ϕ_{FF} and $I(\phi_{\mathrm{FF}})$ are the far-field angle and far-field angular distributions, respectively. As shown in Fig. 1(f), the unidirectional emission quickly reduces with the decrease of α_{m} at $m = 13$, confirming the influences of higher-order components very well. The asymmetric shape of U is caused by the phase differences between components with different radial numbers [46]. Here, we use the $U(170^{\circ}, 190^{\circ})$ instead of $U(180^{\circ}, 180^{\circ})$ to take the divergent light emission into account, which originates from the same output beam around $\phi_{\mathrm{FF}} = 180^{\circ}$.

The above configuration, unfortunately, is usually practically limited in practical applications. Due to the coupling between CW and CCW components, two nearly degenerated modes are generated for the same azimuthal number. Mode 3 in Fig. 1(b) is also associated with a nearly degenerated mode with even symmetry. As illustrated in the bottom panel in Fig. 1(e), while both of its azimuthal and radial numbers are the same as the one in the top panel, its far-field pattern is dominated by two directional output beams instead of unidirectional emission. Such kind of emission is also caused by their higher-order components with $m = 13$. Meanwhile, this mode has a higher Q factor than the mode with unidirectional output, making the unidirectional laser emission hard to excite in the experiment. While special cases can produce unidirectional laser output and high Q simultaneously, usually sophisticated designs are required.

Compared with the fine tuning of the cavity shape, the introduction of $\mathcal{PT}$ symmetry can be a robust way to tailor the resonant modes and thus achieve unidirectional laser emission. Figure 2(a) shows the schematic picture of the $\mathcal{PT}$-symmetric annular microdisk. All the structural parameters are the same as in Fig. 1, except that the gain and loss modulations are periodically introduced along the azimuthal direction (ϕ) following the equation

$$\Delta n = \begin{cases} n_{\mathrm{gain}} = -in''\left[\frac{(l-1/4)\pi}{m} < \varphi < \frac{(l+1/4)\pi}{m}\right] \\ n_{\mathrm{loss}} = in''\left[\frac{(l+1/4)\pi}{m} < \varphi < \frac{(l+3/4)\pi}{m}\right] \end{cases}, \quad (2)$$

where n'' and m are the modulation on imaginary parts of the refractive index and azimuthal number, respectively. According to the mode coupling theory, the presence of $\mathcal{PT}$ symmetry shall affect the coupling between CW waves and CCW waves of the designed WGM. Then the wave numbers of the designed WGM can be expressed as $\beta = \beta_0 \pm ikn''$, where β is the intrinsic wave number without $\mathcal{PT}$ symmetry and κ is the coupling constant. It is easy to see that the imaginary part of the designed WGM bifurcates with an arbitrarily small modulation n''. The other WGMs with different azimuthal numbers experience balanced gain and loss, and their $\mathcal{PT}$ symmetries are hard to break. Then only the WGM with particular azimuthal numbers can lase in the experiment. Different from the circular microdisk, the annular microcavity just has the mirror-reflection symmetry, where the symmetry of the designed WGM can also be excited selectively. The modulation in Eq. (2) only produces a laser from the WGM with odd symmetry. Similarly, the laser with even symmetry can also be excited by rotating the modulation $\pi/4m$ along the azimuthal direction. In this sense, the mode in the top panel of Fig. 1(e) can be excited selectively,even though its Q factor is relatively lower than its nearly degenerated mode.

The above analysis has been numerically confirmed in Fig. 2. Taking the mode in Fig. 1(e) as an example, we set the designed azimuthal number at $m = 17$ and numerically calculated the dependence of real and imaginary parts of β on the external modulation n''. The calculated results are summarized in Fig. 2(b). With the increase of n'', the frequencies of the hybrid modes are nearly degenerated at the same frequency, whereas the imaginary parts are conjugated. The odd mode is totally distributed in the gain regions and lases when $n'' > 0$. Meanwhile, the even mode becomes an absorptive mode and is fully suppressed. Here, the setting of n'' is reasonable and referred to previous studies, where a single-mode $\mathcal{PT}$-symmetry microring laser with similar geometries was experimentally demonstrated [42]. Figure 2(c)

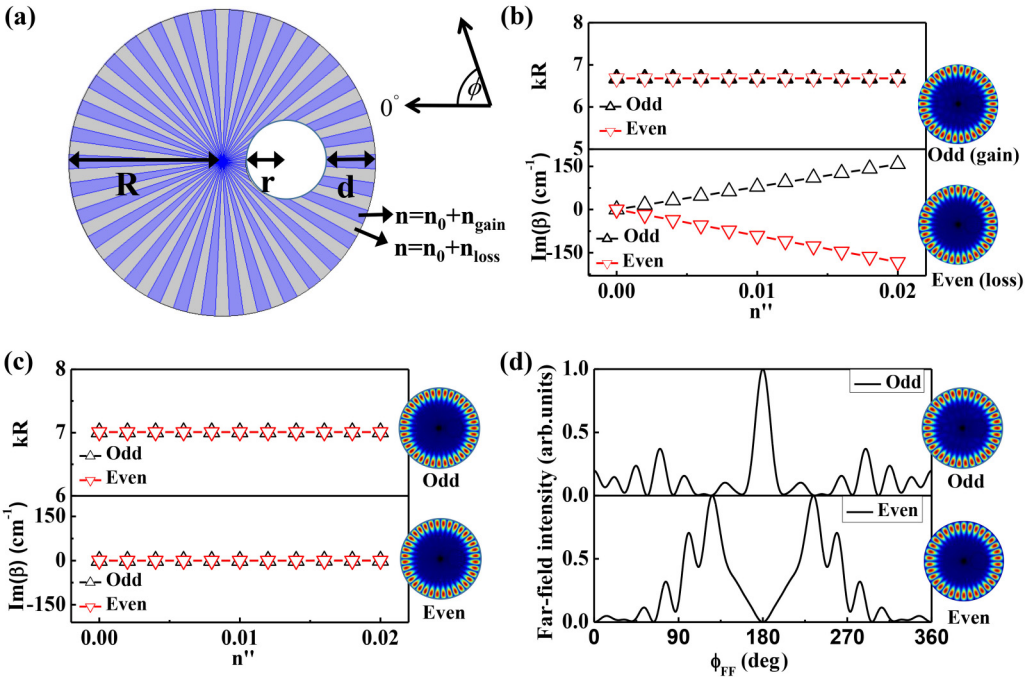

FIG. 2. Mode properties of the $\mathcal{PT}$-symmetric annular microdisk. (a) The schematic of the $\mathcal{PT}$-symmetric microdisk. (b) The real (top panel) and imaginary (bottom panel) wave numbers of designed WGM with $m = 17$ as a function of n''. (c) The dependence of real (top panel) and imaginary (bottom panel) wave numbers of undesigned WGM with $m = 18$ on the modulation n''. (d)The far-field patterns of odd and even modes with $m = 17$ at $n'' = 0.02$.

shows an example with $m = 18$ that illustrates the suppression of undersigned modes. While the real parts of β are still very close, their imaginary parts are kept around 0 even though n'' is already very large. Therefore, while the odd WGM with designed azimuthal number has a relatively lower Q factor in the passive cavity, it can still be excited experimentally by applying $\mathcal{PT}$ symmetry. Figure 2(d) depicts the far-field patterns of the odd and even modes with $m = 17$ at $n'' = 0.02$, respectively. The gain odd mode supports unidirectional output, indicating the unidirectional laser emission in the real experiment. On the contrary, the absorptive even mode cannot lase.

III. UNIDIRECTIONAL EMISSION OF THE CIRCULAR CAVITY WITH A POINT SCATTER

The selection of the special mode with $\mathcal{PT}$ symmetry is quite generic in an optical microcavity and it can further improve the unidirectionality. One example is the microdisk with a point scatter inside [see Fig. 3(a)]. Here the point scatter is set at $r = 0.01R$, $n = 3$, and $d = 0.48R$. The other parameters are the same as in Fig. 1. Figure 3(b) shows the Q factors of the calculated resonances, where a series of high-Q modes can be clearly seen. According to their field patterns, these modes have also been marked with their azimuthal number and radial number (m, l). The modes with small radial numbers are typically confined along the cavity boundary and less affected by the point scatter. Thus their Q factors can be higher than 10^{10} and their far-field patterns are nearly isotropic [bottom panel in Fig. 3(c)]. However, the properties of some high-order modes are quite different. For example, as the mode WGM (20, 4) in Fig. 3(b) has strong field distributions at the point scatter, the corresponding electromagnetic fields are strongly scattered, due to the large refractive index contrast. According to the Huygens-Fresnel principle, the curved cavity surface could work as a focusing lens. By precisely designing the scatter's position, the incident plane wave can be focused at the point scatter and then coupled into the WGMs. In this sense, following the time-reversal process, the scattered light from WGM (20, 4) shall be collected by the microdisk and collimated into a highly directional beam in the far field. The corresponding far-field pattern is plotted in the top panel of Fig. 3(c), where a single beam with a divergence angle $\sim 10^\circ$ is observed. Such kind of highly unidirectional emission is essential for practical applications. However, since its Q factors are orders of magnitude lower, such mode is impossible to be excited with a conventional method. Then the laser emissions are determined by the other high-Q modes with nearly isotropic emissions [see Fig. 3(d)]. Compared with the annular cavity, the Q factors, as well as the formation of high directionality U, are quite different. The corresponding quantitative comparisons of the two cavities are shown in Appendix A. To restrain the high-Q modes with isotropic emissions, we have also introduced the $\mathcal{PT}$ symmetry along the azimuthal direction to generate the unidirectional single-mode laser emission (see Appendix B).

IV. UNIDIRECTIONAL EMISSION WITHOUT MODULATION ON THE REAL PART OF THE REFRACTIVE INDEX

More than the selection of particular modes with unidirectional output, the $\mathcal{PT}$ symmetry can also be applied to a conventional circular microdisk (without any deformation and internal structures) to tailor the internal ray dynamics and

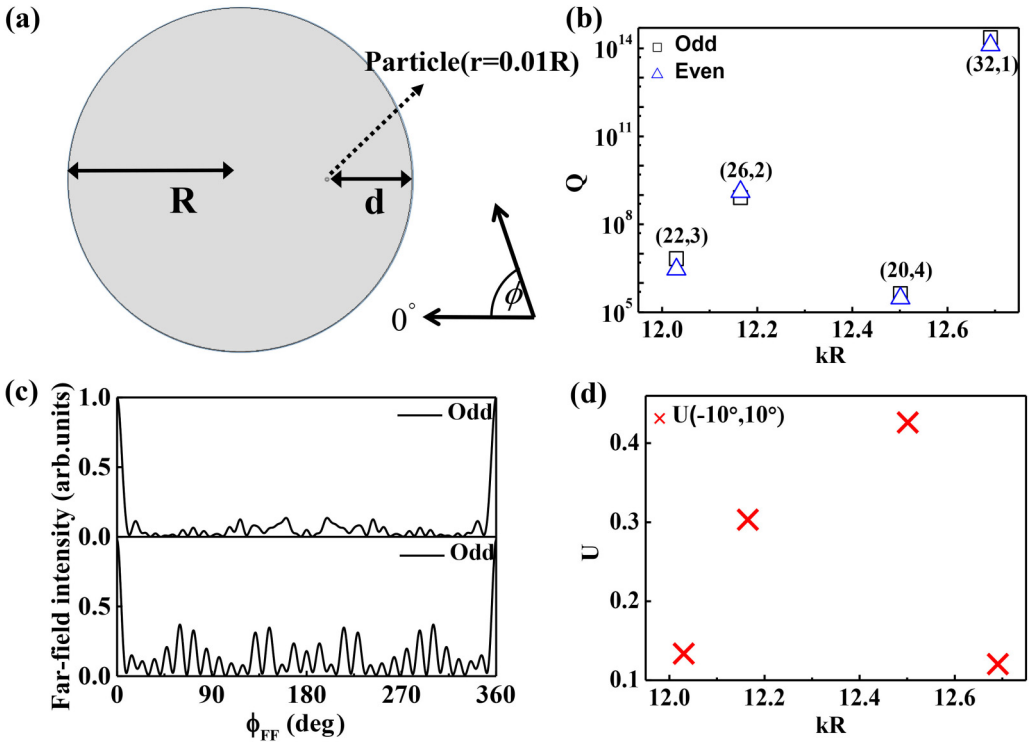

FIG. 3. Resonances in the microdisk with a point scatter. (a) The schematic picture of the microdisk with a point defect. (b) The resonant modes inside the microdisk with a point defect. (c) The far-field angular distributions of WGM (20, 4) (top panel) and WGM (32, 1) (bottom panel). (d) The $U(\theta_1, \theta_2)$ factor of the resonances in (b). Here $U(\theta_1, \theta_2)$ follows the same definition as in Fig. 1.

generate unidirectional output. This research area, however, has not been considered in previous reports. Figure 4(a) shows the schematic picture of the $\mathcal{PT}$-symmetric microdisk. The real part of the refractive index of the circular microdisk is uniformly defined as $n_0 = 3.3$. The imaginary part of the refractive index is periodically modulated along the azimuthal direction. The primary setting is similar to Fig. 2, where the gain and loss are periodically modulated following Eq. (2) along the azimuthal direction. In additional to the main modulation, there is also a small circle with radius $r = 0.31R$. The minimal distance between the two disks is $d = 0.6R$. The modulation on n'' is also periodic in the small circle, but its gain and loss regions are completely reversed to the big circle. For such kind of $\mathcal{PT}$-symmetric modulations, the resonance with designed azimuthal number and symmetry ($m = 18$, odd symmetry) has been studied and summarized in Fig. 4(b). With the increase of n'', the frequencies of WGMs with designed azimuthal number are nearly degenerated [top panel in Fig. 4(b)]. The imaginary parts, which relate to laser and absorption modes, bifurcate rapidly when n'' is above 0 in the bottom panel of Fig. 4(b). While the $\mathcal{PT}$-symmetry breaking can also happen in undersigned modes, their gain coefficients are almost an order of magnitude lower and thus cannot be excited. All of these phenomena are consistent with the thresholdless $\mathcal{PT}$-symmetry breaking.

In additional to the $\mathcal{PT}$-symmetry breaking, its influences on the directionality are more interesting for both fundamental research and practical applications. In a circular cavity with uniform refractive index distribution ($n = 3.3$), the WGMs are confined along the regular ray dynamics. Such modes typically have extremely high Q factors and isotropic emissions [see Fig. 4(d)]. In contrast, when an air hole is drilled inside the microdisk, the ray dynamics can be significantly changed by the inner boundary and unidirectional emission is formed [Fig. 4(e)]. However, the Q factors are also strongly spoiled. For the case of a $\mathcal{PT}$-symmetric microdisk in Fig. 4(a), it shows totally different behaviors. In the case of $n'' = 0$, the resonant modes are conventional WGMs with extremely high Q factors, indicating that the threshold of the potential laser shall be very small even though the material losses are considered. When $n'' = 0.001$, the $\mathcal{PT}$ symmetry is broken and the far-field pattern also changes dramatically. As shown in Fig. 4(c), here the output is dominated by one beam around $\phi_{\mathrm{FF}} = 0^\circ$ instead of isotropic output. The divergence angle in Fig. 4(c) is as small as 15° and the other emissions are orders of magnitude smaller. Interestingly, the unidirectional emission is found to be robust to the increase of n''. It stays almost the same at $n'' = 0.01$ in Fig. 4(c). Figure 4(f) summarizes the dependence of the U factor on the external modulation. We can see that the highly unidirectional emission is quite robust after the $\mathcal{PT}$-symmetry breaking. Considering the symmetry of a circular microcavity and its regular ray dynamics, the unidirectional emission in Fig. 4 clearly demonstrates that two sets of $\mathcal{PT}$-symmetric modulations have strong impacts on the internal ray dynamics of a circular microcavity. In addition, the unidirectional emission is not limited in the high-refractive-index material. On the contrary, this mechanism is quite robust to the refractive index. As shown in Appendix C, the unidirectional emission is also obtained with $n = 1.56$ (for a dyed polymer).

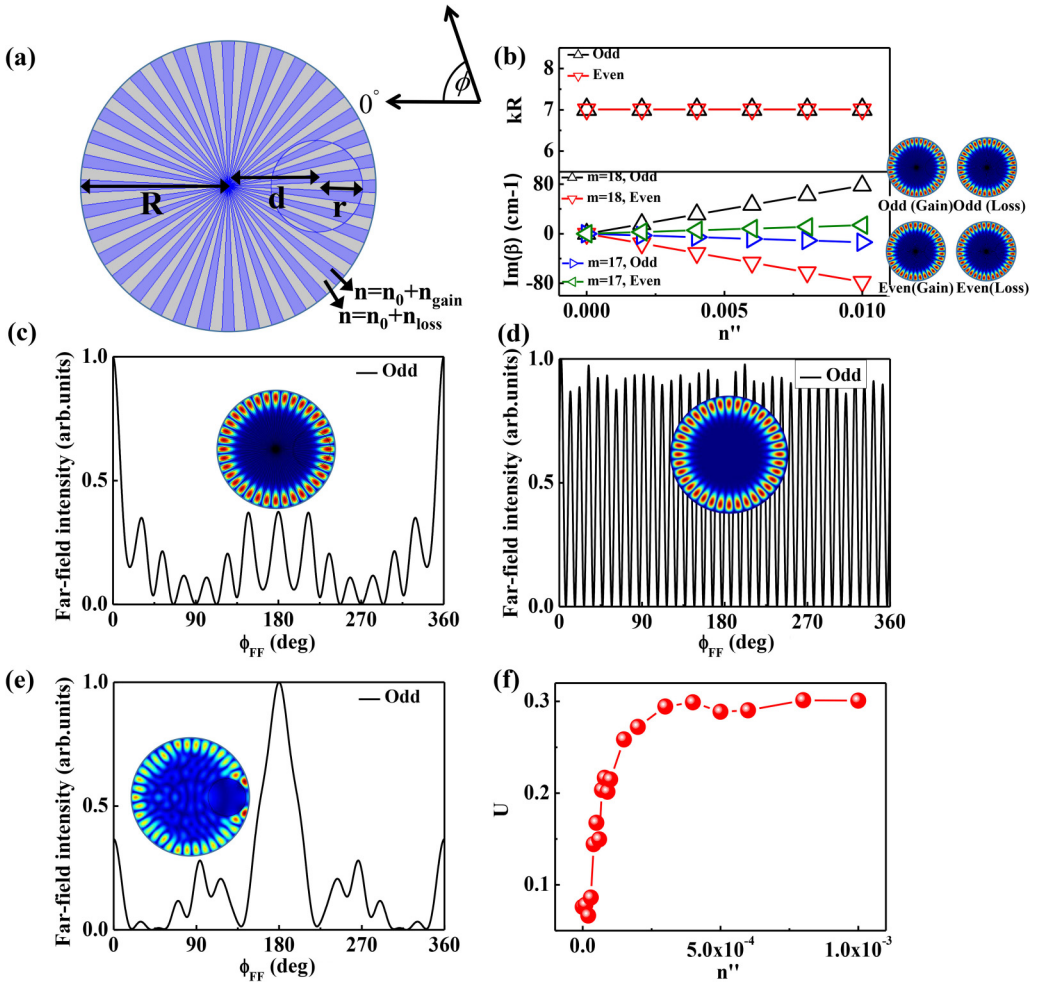

FIG. 4. Resonances in the $\mathcal{PT}$-symmetric microdisk without any deformation. (a) Schematic picture of the undeformed $\mathcal{PT}$-symmetric microdisk. (b) The upward and downward triangles are the real and imaginary parts of resonant frequencies as a function of n''. The undersigned modes are plotted as left- and right-pointing triangles. (c) The far-field pattern of the designed mode with $m = 18$ at different n''. (d) The near-field and far-field patterns of the WGM with $m = 18$ in the circular cavity without $\mathcal{PT}$ symmetry. Here the kR of the mode is 7.695. (e) The near-field and far-field patterns of the WGM with $m = 18$ in the annular cavity with an air hole inside. Here the kR of the mode is 7.26. (f) The dependence of the U (–10°, 10°) factor on the modulation n''.

V. CONCLUSION

In summary, we have studied the influences of $\mathcal{PT}$ symmetry on the directionality of microdisk lasers. In an annular microcavity and a microdisk with a point defect, we show that the $\mathcal{PT}$ symmetry can be applied to select a particular mode with defined symmetry. As a result, single-mode and unidirectional laser emissions have been simply achieved even though the original modes have relatively lower Q factors in passive cavities. More interestingly, we find that the $\mathcal{PT}$-symmetric modulations on the imaginary parts of the refractive index in a circular microdisk can affect the internal ray dynamics. By controlling the distributions of two sets of $\mathcal{PT}$-symmetric modulations, highly directional output in a single direction has also been generated after the $\mathcal{PT}$-symmetry breaking. This research shall play important roles in the reconsideration of ray dynamics inside optical microdisks and their practical applications [47,48].

ACKNOWLEDGMENTS

The authors would like to express thanks for the financial support from the Shenzhen Fundamental Research Projects (Project No. JCYJ20160427183259083), the Public Platform for Fabrication and Detection of Micro- and Nano-sized Aerospace Devices, and Shenzhen Engineering Laboratory on Organic-Inorganic Perovskite Devices.

D.Z. and S.L. contributed equally to this work.

APPENDIX A: COMPARISON BETWEEN THE ANNULAR CAVITY AND THE SCATTER CAVITY

In the main manuscript, we have discussed the formation of unidirectional emission of annular and scatter cavities individually. In this Appendix, we will give quantitative comparisons of these cavities. For the annular cavity, the combination of high Q factor and high unidirectionality results

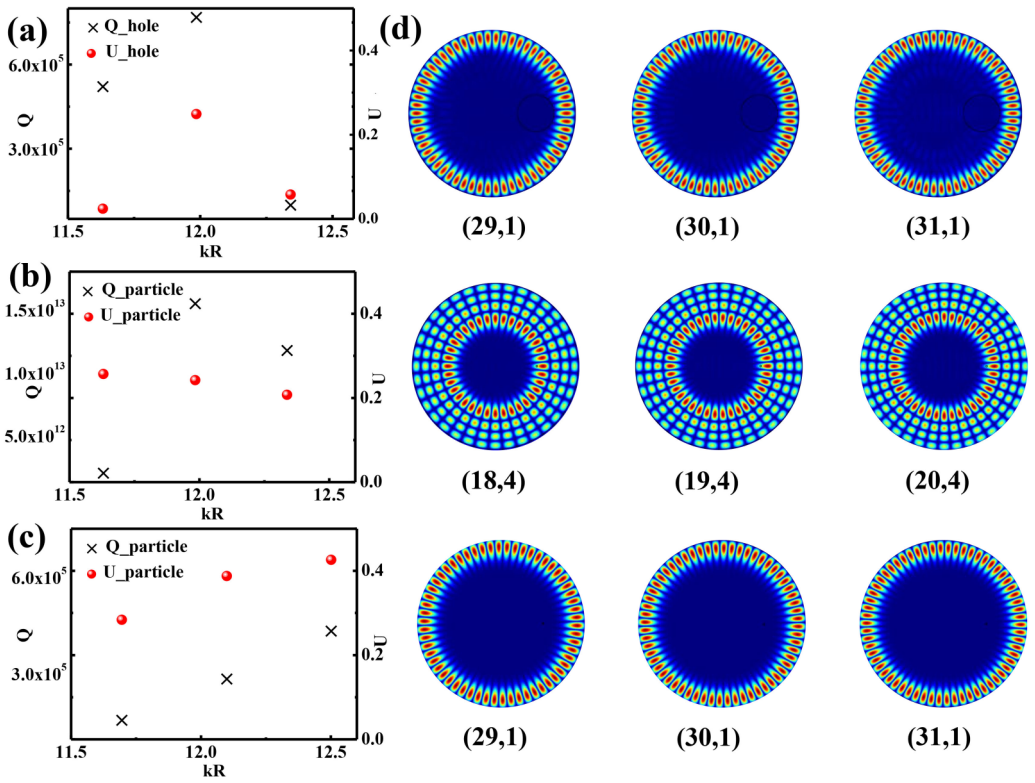

FIG. 5. The comparisons between the annular cavity and the scatter cavity. (a) Q factor and unidirectionality of fundamental modes in the annular cavity. (b) Q factor and unidirectionality of the high-order modes in the scatter cavity. (c) Q factor and unidirectionality of the fundamental modes in the scatter cavity. (d) The corresponding field distributions of the modes marked in (a,b,c), respectively.

from the mode coupling between a high-Q fundamental mode and low-Q high-order modes, which is obviously shown in Figs. 1(d) and 1(f). The high-Q fundamental mode could support the high Q factor, whereas the low-Q high-order modes are reflected at the boundary of the inner circle and thus provide high directionality around $\phi_{\mathrm{FF}} = 180^{\circ}$. When their coupling strength is strong enough [corresponding to high α_m in Fig. 1(f)], the low-Q high-order modes will dominate the directionality. As a result, the unidirectional emission around $\phi_{\mathrm{FF}} = 180^{\circ}$ is demonstrated, which is shown in Fig. 1(e). As a comparison, the formation of unidirectionality in the scatter cavity is significantly different. When the particle is located at the focus point of the curved cavity surface, the high-order WGMs are strongly scattered and then generate the high directionality around $\phi_{\mathrm{FF}} = 0^{\circ}$. The unidirectionality could be explained by its time-reversal process, where the incident light from $\phi_{\mathrm{FF}} = 0^{\circ}$ is focused by the curved cavity boundary on the scattering particle. However, the low-order modes have stronger confinement along the radial direction and are barely affected by the scattering point, so these modes show high Q factors but isotropic emission.

The modes of Figs. 1(f) and 3(d) have a large difference in kR. Next, we will fix kR around $kR \sim 12$. The other parameters are the same as in the main manuscript. Figure 5 shows the calculated Q factors, directionality U, and the corresponding field distributions of the annular and scatter cavity, respectively. The three nearby modes in Fig. 5(a) are the fundamental WGMs, where the corresponding field distributions are shown in Fig. 5(d). Here, $r = 0.22R$ and $d = 0.525R$. We can see all of the three modes keep high Q factors, but quite different directionality U. As we mentioned above, the fundamental WGMs could couple with the nearby high-order modes, which will dominate the directionality as well as decrease the Q factors. Consequently, although WGM (29,1), WGM (30,1), and WGM (31,1) have similar field distributions, their far-field emissions are totally different. For WGM (30,1), the coupled high-order modes have relative high U around $\phi_{\mathrm{FF}} = 180^{\circ}$ and high Q factors. However, for WGM (31,1), the coupled high-order modes have a reverse far-field emission around $\phi_{\mathrm{FF}} = 0^{\circ}$ and low Q factors. That is the reason that WGM (30,1) could maintain the maximal Q and U.

As shown in Fig. 5(b), the Q factors of the scatter cavity are generally smaller than the annular cavity. However, the directionality is quite robust. Here, we fix $r = 0.01R$ and $d = 0.48R$. The difference in U [shown in Fig. 5(b)] could be understood as the following process: For a circular microdisk with fixed R, different kR relates to the different focusing position. In our simulation, the scatter is designed at the focusing point of $kR \sim 12.5$, which exactly corresponds to the resonant wavelength of WGM (20,4). Therefore, the light of WGM (20,4) could scatter and propagate along the inverse focusing path effectively. For the other modes, the U decreases as the scatter is far away from their optimal focusing point. But, in a wide range, the scatter cavity remains highly unidirectional (maximal $U = 0.426$), which is clearly shown in Fig. 5(b). As a comparison, Fig. 5(c) shows the three fundamental WGMs of the scatter cavity. These modes have

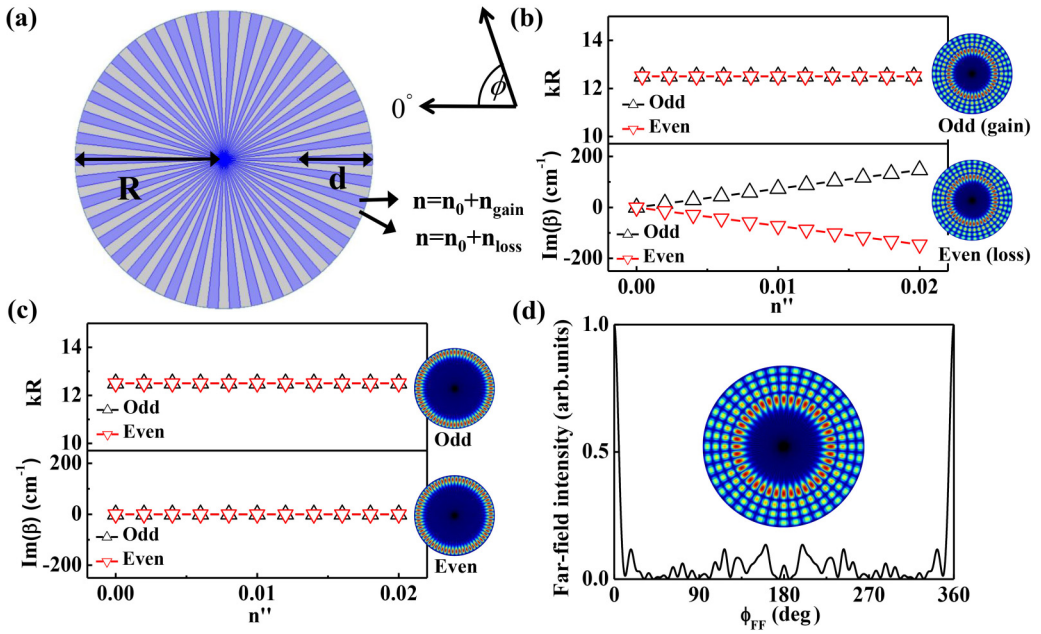

FIG. 6. Resonances in the $\mathcal{PT}$-symmetric microdisk with a point scatter. (a) The schematic picture of the $\mathcal{PT}$-symmetric microdisk. (b) The real (top panel) and imaginary (bottom panel) wave numbers of the designed WGM with $m = 20$ as a function of n''. (c) The dependence of real (top panel) and imaginary (bottom panel) wave numbers of the undesigned WGM with $m = 32$ on the modulation n''. (d) The far-field pattern of the odd mode with $m = 20$ at $n'' = 0.02$.

stronger confinement along the radial direction and are barely affected by the scattering point, which is obviously shown in the field distributions of Fig. 5(d), so these modes show high Q factors (more than 10^{11}). Meanwhile, the far-field emission is nearly isotropic. The directionality U of all three modes is less than 0.26.

APPENDIX B: RESONANCES IN THE $\mathcal{PT}$-SYMMETRIC MICRODISKWITH A POINT SCATTER

In this Appendix, we demonstrate the unidirectional emission of the $\mathcal{PT}$-symmetric microdisk with a point scatter. All the settings are the same as in Fig. 2(a) in the main manuscript, except that the azimuthal number is set as $m = 20$. Figure 6(b) shows the real parts and imaginary parts of β as a function of the modulation n''. Similar to the results in Fig. 2, a thresholdless $\mathcal{PT}$-symmetry breaking can be observed clearly. With the increase of n'', the frequencies of two hybrid modes nearly degenerate. and the corresponding imaginary parts of β bifurcate quickly. One mode becomes lossier and the other one starts to lase. Similarly, even though the undesigned modes have much higher Q factors for the passive cavity, they will experience balanced gain and loss in the $\mathcal{PT}$-symmetric microdisk and their $\mathcal{PT}$ symmetry cannot be broken [see Fig. 6(c)]. Then their imaginary parts are well kept around 0 during the increase of n''. In this sense, only the WGMs with designed azimuthal number and symmetry can be selectively excited in experiments. Figure 6(d) shows the corresponding far-field angular distribution, which is exactly the same as the one in the passive cavity without $\mathcal{PT}$ symmetry [Fig. 3(c)]. Therefore, by applying $\mathcal{PT}$ symmetry, the microdisk with a point scatter can be used to generate a single-mode laser with a highly unidirectional output.

APPENDIX C: UNIDIRECTIONAL EMISSION OF LOW-REFRACTIVE-INDEX $\mathcal{PT}$-SYMMETRY MICRODISK

As shown in Fig 4, the improvement of unidirectionality of the circular microdisk with a designed $\mathcal{PT}$-symmetric structure has been identified. However, the unidirectional emission is not a particular case for a high-refractive-index material. In this Appendix, we will demonstrate that the high unidirectionality is maintained even with a low-refractive-index material. Here, we take the SU8 dyed with rhodamine B (corresponding to $n_0 = 1.56$) as an example. Figure 7 depicts the corresponding schematic picture. The radius of the inner circle and offset distance are set as $r = 0.4R$ and $d = 0.54R$, respectively. From the far-field pattern in Fig. 7(b), we can clearly see the unidirectional emission of odd WGM (35,1) with $n'' = 0.02$.

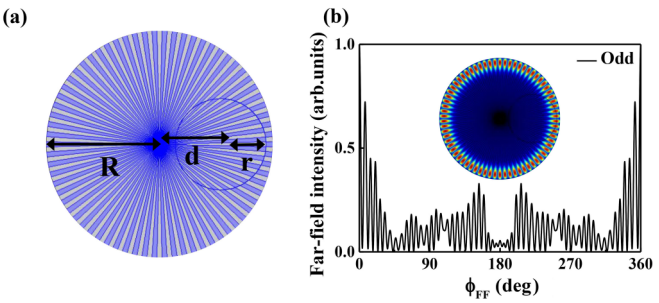

FIG. 7. Unidirectional emission of the low-refractive-index $\mathcal{PT}$-symmetric microdisk. (a) Schematic picture of the low-refractive-index $\mathcal{PT}$-symmetric microdisk. The period number of loss modulation is 35. (b) The far-field pattern of the designed odd WGM (35,1). Inset is the corresponding field distributions.

[1] K. J. Vahala, Nature (London) **424**, 839 (2003).
[2] A. Ishii, X. He, N. F. Hartmann, H. Machiya, H. Htoon, S. K. Doorn, and Y. K. Kato, Nano Lett. **18**, 3873 (2018).
[3] A. Orieux, M. A. M. Versteegh, K. D. Jons, and S. Ducci, Rep. Prog. Phys. **80**, 076001 (2017).
[4] A. Bhattacharya, M. Z. Baten, I. Iorsh, T. Frost, A. Kavokin, and P. Bhattacharya, Phys. Rev. B **94**, 035203 (2016).
[5] Y. J. Lee, D. E. Lee, and S. H. Kwon, IEEE Photon. J. **9**, 1 (2017).
[6] Z. X. Xiao, Y. Z. Huang, Y. D. Yang, M. Tang, and J. L. Xiao, Opt. Lett. **42**, 3173 (2017).
[7] A. Dreismann, H. Ohadi, Y. del Valle-Inclan Redondo, R. Balili, Y. G. Rubo, S. I. Tsintzos, G. Deligeorgis, Z. Hatzopoulos, P. G. Savvidis, and J. J. Baumberg, Nat. Mater. **15**, 1074 (2016).
[8] K. Y. Wang, G. Li, S. Wang, S. Liu, W. Z. Sun, C. Huang, Y. J. Wang, Q. H. Song, and S. M. Xiao, Adv. Mater. **30**, 1801481 (2018).
[9] B. B. Li, W. R. Clements, X. C. Yu, K. Shi, Q. H. Gong, and Y. F. Xiao, Proc. Natl. Acad. Sci. USA **111**, 14657 (2014).
[10] S. J. Tang, S. Liu, X. C. Yu, Q. H. Song, Q. H. Gong, and Y. F. Xiao, Adv. Mater. **30**, 1800262 (2018).
[11] J. Wiersig, Phys. Rev. Lett. **112**, 203901 (2014).
[12] W. J. Chen, S. K. Ozdemir, G. M. Zhao, J. Wiersig, and L. Yang, Nature **548**, 192 (2017).
[13] F. Vollmer, D. Braun, and A. Libchaber, Appl. Phys. Lett. **80**, 4057 (2002).
[14] J. Zhu, Ş. K. Özdemir, Y.-F. Xiao, L. Li, L. He, D.-R. Chen, and L. Yang, Nat. Photon. **4**, 46 (2010).
[15] Y. J. Wang, N. Zhang, Z. Q. Jiang, L. Wang, Y. F. Xiao, W. Z. Sun, N. B. Yi, S. Liu, X. Gu, S. M. Xiao, and Q. H. Song, Adv. Mater. Technol. **2**, 1600299 (2017).
[16] D. Armani, B. Min, A. Martin, and K. J. Vahala, Appl. Phys. Lett. **85**, 5439 (2004).
[17] J. S. Levy, A. Gondarenko, M. A. Foster, A. C. Turner-Foster, A. L. Gaeta, and M. Lipson, Nat. Photon. **4**, 37 (2010).
[18] N. Zhang, Z. Y. Gu, S. Liu, Y. J. Wang, S. Wang, Z. H. Duan, W. Z. Sun, Y. F. Xiao, S. M. Xiao, and Q. H. Song, Optica **4**, 1151 (2017).
[19] Q. H. Song, H. Cao, S. T. Ho, and G. S. Solomon, Appl. Phys. Lett. **94**, 061109 (2009).
[20] X.-F. Jiang, Y.-F. Xiao, C.-L. Zou, L. He, C.-H. Dong, B.-B. Li, Y. Li, F.-W. Sun, L. Yang, and Q. Gong, Adv. Mater. **24**, OP260 (2012).
[21] B. Min, L. Yang, and K. J. Vahala, Appl. Phys. Lett. **87**, 181109 (2005).
[22] S. M. Spillane, T. J. Kippenberg, and K. J. Vahala, Nature **415**, 621 (2002).
[23] K. Y. Wang, Z. Y. Gu, S. Liu, W. Z. Sun, N. Zhang, S. M. Xiao, and Q. H. Song, J. Phys. Chem. Lett. **7**, 2549 (2016).
[24] N. Zhang, W. Z. Sun, S. P. Rodrigues, K. Y. Wang, Z. Y. Gu, S. Wang, W. S. Cai, S. M. Xiao, and Q. H. Song, Adv. Mater. **29**, 1606205 (2017).
[25] Z. H. Duan, Y. J. Wang, G. Li, S. Wang, N. B. Yi, S. Liu, S. M. Xiao, and Q. H. Song, Laser Photon. Rev. **12**, 1700234 (2018).
[26] H. Cao and J. Wiersig, Rev. Mod. Phys. **87**, 61 (2015).
[27] Q. H. Song, L. Ge, B. Redding, and H. Cao, Phys. Rev. Lett. **108**, 243902 (2012).
[28] G. D. Chern, H. E. Tureci, A. D. Stone, and R. K. Chang, Appl. Phys. Lett. **83**, 1710 (2003).
[29] V. M. Apalkov and M. E. Raikh, Phys. Rev. B **70**, 195317 (2004).
[30] J. Wiersig and M. Hentschel, Phys. Rev. A **73**, 031802 (2006).
[31] C. P. Dettmann, G. V. Morozov, M. Sieber, and H. Waalkens, Phys. Rev. A **80**, 063813 (2009).
[32] Q. J. Wang, C. L. Yan, N. F. Yu, J. Unterhinninghofen, J. Wiersig, C. Pflügl, L. Diehl, T. Edamura, M. Yamanishi, H. Kan, and F. Capasso, Proc. Natl. Acad. Sci. USA **107**, 22407 (2010).
[33] Q. H. Song and H. Cao, Opt. Lett. **36**, 103 (2011).
[34] M. Bender, P. H. Heenen, and P. G. Reinhard, Rev. Mod. Phys. **75**, 121 (2003).
[35] L. Ge and A. D. Stone, Phys. Rev. X **4**, 031011 (2014).
[36] B. Peng, Ş. K. Özdemir, F. Lei, F. Monifi, M. Gianfreda, G. L. Long, S. H. Fan, F. Nori, C. M. Bender, and L. Yang, Nat. Phys. **10**, 394 (2014).
[37] R. El-Ganainy, K. G. Makris, M. Khajavikhan, Z. H. Musslimani, S. Rotter, and D. N. Christodoulides, Nat. Phys. **14**, 11 (2018).
[38] Y. D. Chong, Li Ge, and A. D. Stone, Phys. Rev. Lett. **106**, 093902 (2011).
[39] Z. Lin, H. Ramezani, T. Eichelkraut, T. Kottos, H. Cao, and D. N. Christodoulides, Phys. Rev. Lett. **106**, 213901 (2011).
[40] M. A. Miri, P. LiKamWa, and D. N. Christodoulides, Opt. Lett. **37**, 764 (2012).
[41] A. Regensburger, C. Bersch, M. Miri, G. Onishchukov, D. N. Christodoulides, and U. Peschel, Nature **488**, 167 (2012).
[42] L. Feng, Z. J. Wong, R. M. Ma, Y. Wang, and X. Zhang, Science **346**, 972 (2014).
[43] H. Hodaei, M. A. Miri, M. Heinrich, and D. N. Christodoulides, Science **346**, 975 (2014).
[44] Z. Y. Gu, N. Zhang, Q. Lyu, M. Li, S. M. Xiao, and Q. H. Song, Laser Photon. Rev. **10**, 588 (2016).
[45] L. Chang, X. Jiang, S. Hua, C. Yang, J. Wen, L. Jiang, G. Li, G. Wang, and M. Xiao, Nat. Photon. **8**, 524 (2014).
[46] L. Ge, Q. H. Song, B. Redding, and H. Cao, Phys. Rev. A **87**, 023833 (2013).
[47] Q. H. Song, L. Ge, A. D. Stone, H. Cao, J. Wiersig, J.-B. Shim, J. Unterhinninghofen, W. Fang, and G. S. Solomon, Phys. Rev. Lett. **105**, 103902 (2010).
[48] X. F. Jiang, L. B. Shao, S. X. Zhang, X. Yi, J. Wiersig, L. Wang, Q. H. Gong, M. Lončar, L. Yang, and Y. F. Xiao, Science **358**, 344 (2017).